For: Proceedings of the 5th International Conference on Gas Hydrates, Trondheim, Norway, June 2005

Rheological comparisons and structural imaging of sI and sII end-member gas hydrates and hydrate/sediment aggregates.

William Durham
U.C. Lawrence Livermore National Laboratory
Livermore, CA, 94550, USA

Laura Stern*, Stephen Kirby, and Susan Circone
U.S. Geological Survey, MS/ 977
Menlo Park, CA, 94025, USA

ABSTRACT

We report the results of exploratory measurements on the plastic yield strength of fully dense methane hydrate + quartz sand aggregates, and CO_2 hydrate + quartz sand aggregates, at conditions relevant to hydrate-bearing environments on Earth. We compare these results to those measured previously on pure end-member gas hydrates (sI methane hydrate, sI CO_2 hydrate, and sII methane-ethane hydrate) as well as to pure water ice and to ice + sand aggregate mixtures. All gas hydrates we have tested to date are exceptionally strong relative to ice, and hence may serve to increase the strength and cohesion of hydrate-bearing sediments significantly more than previously predicted. Lastly, we use cryogenic scanning electron microscopy (SEM) imaging techniques to examine the phase distribution, grain morphology, grain contacts, and textural evolution within the samples.

Keywords: gas hydrate rheology, flow strength, scanning electron microscopy

INTRODUCTION AND BACKGROUND

A number of factors govern the response of natural gas-hydrate-bearing formations to gravitational, tectonic, and/or man-made forces, including the mechanical strength and rheology of hydrate, the hydrate concentration and geometric distribution of the phases present, and the cohesion and frictional resistance between grains. Hydrate concentrations may be as low as 1-2 vol. % in marine sediments [1], or as high as several tens of percent in permafrost regions [2]. In deposits where hydrate is located structurally between sediment grains or as cement around contacting grains, grain-to-grain cohesion and frictional resistance, from which unconsolidated soft sediments derive their strength [3], can be affected. Even at low concentrations, intergranular hydrate may thus influence formation strength depending on its articulation within the sediment host. At higher concentrations, we may expect a formation–strengthening effect from pore-filling gas hydrate by analogy to strength enhancement in frozen soils [4] or from general theory and experiment with rheologies of aggregate mixtures [5, 6].

Gas hydrate decomposition may also affect formation strength. For example, decomposition is endothermic, and at temperatures above 0°C is rate-controlled by heat flow [7, 8]. Where hydrate exists near the limit of its stability, even small increases in temperature may destabilize it. Not only are any strengthening effects of the hydrate then lost due to loss of material and cohesion, but this weakening effect is in addition to the pore-pressure effect of gas release. These many properties and effects, in addition to those introduced by the environmental pore pressure conditions, place severe limits on the conditions under which gas hydrates may be stable in nature.

Corresponding author. E-mail: lstern@usgs.gov

Volumetric proportions and arrangements of the hydrate phase relative to the sediment matrix in natural formations are often poorly known, however, due to the difficulties in determining the *in situ* location and distribution of phases in partially decomposed material retrieved as drill core. Until recently, evaluating the effects of hydrocarbon hydrates on sediment properties was further complicated because many of the fundamental physical properties had not been directly measured on pure end-member gas hydrates, and particularly methane hydrate, thought to be the principal hydrocarbon in natural hydrates. Ordinary water ice and gas hydrates share similarities in the nature of the hydrogen-bonding forming the framework of their open structures, and many of the material properties of ice have thus commonly been used in lieu of direct measurements on hydrocarbon hydrates. This assumption seems reasonable at first glance, given that gas hydrates are approximately 85 mol % water even with all cages occupied [9] and given the close similarity in water molecule hydrogen-bond lengths (~ 1% larger in gas hydrates than ice) and oxygen-bond angles (~ 3.5° larger in hydrates than ice).

In the case of mechanical properties, however, this assumption is now known to be wrong. Several lines of experimental evidence reveal that end-member clathrate hydrates tested to date are in fact *exceptionally* strong relative to ice, and hence may serve to increase the strength and cohesion of hydrate/sediment formations more than previously expected. (**1**) Hydrostatic and uniaxial compaction experiments on pure, gas-saturated porous hydrate indicate that effective pressures approaching 100 MPa are required to fully compact sI methane hydrate and sII methane-ethane hydrate [10-14], even at temperatures well above the ice melting line where the mobility of water molecules should be very high. This compares with the easy compaction of granular ice at pressures of only several tens of MPa at –5°C [13, 14]. This difference cannot be explained by the minimal pore pressure required to keep gas hydrate stable during compaction. (**2**) Triaxial compression tests indicate that sI methane hydrate, sI CO_2 hydrate, and sII methane-ethane hydrate all have ductile flow strengths that are 20 to upward of 100 times stronger than ice under the same conditions [10-12]. (**3**) Porous hydrates, compacted hydrates, and hydrate / sand aggregates synthesized in our laboratory are found to be significantly more cohesive and durable than comparable granular ice, compacted ice, and ice/sand aggregates. This observation is also consistent with experience in drill coring of hydrate/sand intervals compared with ice/sand intervals. These findings also suggest that the effects of gas hydrate in increasing the strength of sediments is considerably larger than the effects of ice in permafrost. Such strengthening would then be lost during thermal decomposition, and it is important to note that this weakening is in addition to a potentially large pore-pressure effect of gas release.

Here, we report the results of recent exploratory measurements of the plastic yield strength of fully dense samples of methane hydrate + quartz sand and CO_2 hydrate + sand, at conditions relevant to hydrate-bearing environments on Earth. Synthesis, compaction, and rheological testing methods have been developed and reported previously by our group [10, 15-17] and are only briefly reviewed here. We compare the strength of the hydrate/aggregate mixtures to those measured previously on pure end-member gas hydrates [10-12], ice [18], and ice + quartz sand aggregates [19]. Lastly, we use cryogenic scanning electron microscopy (SEM) imaging techniques to examine the phase distribution, grain morphologies, grain contacts, and microstructural development within the samples. Such textural information not only aids in the interpretation of the experimental results, but also helps relate the measurements to previously reported observations and/or to rock-physics models of hydrate-bearing sediment assemblages.

EXPERIMENTAL METHODS

Sample synthesis. Samples of pure, polycrystalline gas hydrates, including sI methane hydrate, sI CO_2 hydrate, and sII methane-ethane hydrate, were synthesized by warming granulated (~ 200 μm) ice under static conditions in an atmosphere pressurized by the hydrate-forming gas or liquid of interest (see [15-17] for further details). Full reaction of 30 g of ice to hydrate in each of these cases typically can be completed within 10 to 20 hours at high temperature (T) and high pressure (P) conditions deep within the stability field of the appropriate hydrate. Complete reaction is confirmed by the absence of a P-T discontinuity when samples are subsequently cooled to T below the ice melting line (Fig. 3 in [16]). X-ray and

neutron diffraction were also used to verify sample purity (Fig. 3A in [17] for example) and stoichiometry was measured using a custom flow meter and gas collection apparatus [20]. Compositions of final "as-grown" materials, are: $CH_4 \cdot 5.89\ H_2O$ for methane hydrate, $CO_2 \cdot 5.8H_2O$ for C O_2 hydrate, and $(0.82CH_4+0.18C_2H_6) \cdot 5.67H_2O$ for sII methane-ethane hydrate formed from a source gas of composition 0.91:0.09 methane:ethane.

Synthesis of hydrate/sediment aggregates involved simple pre-mixing of sediment particles with the granular ice in the reaction vessel prior to admitting hydrate-forming gas. Minimal migration of either H_2O or sediment grains accompanies reaction, allowing fabrication of homogeneous samples with pre-selected mixing or layering sequences (shown in Fig. 4 in [16]). Alternatively, sediment can be mixed with pure hydrate grains inside a supporting soft-metal container, and then hydrostatically pressurized to a dense, mechanically competent material. For all samples here in which sand was added, we used standard quartz sand (Oklahoma #1, 125 ± 50μm). Synthesis of polycrystalline ice samples and ice/ sand aggregates is described in [19].

Mechanical testing. For compaction and rheological testing of gas hydrates and/or ice, we used a triaxial gas apparatus and standard rock mechanics methods, including encapsulated samples sealed against gas entry, and elevated confining pressures to suppress macroscopic fracture [10]. The apparatus is a 0.6 GPa gas deformation apparatus outfitted for cryogenic use. N_2 or He gas provides the external confining medium, and the pressurized loading column consists of a vented internal force gauge, the jacketed sample, and a moving piston that compresses the sample axially. A pore pressure line communicates gas pressure to the sample and ensures maintenance of the hydrate within its equilibrium stability field throughout testing. Samples were tested at confining pressures of 50 and 100 MPa, pore pressures of 1.6 to 15 MPa (depending on hydrate composition), temperatures ranging $260 \le T \le 287$ K, and differential stresses of $5.7 \le \sigma \le 51.7$ MPa (Fig. 1). Following testing, samples were cooled slowly under pressure to T below 150 K, then further cooled, depressurized, and stored in LN for subsequent imaging by SEM.

SEM procedures. Samples were prepared for SEM imaging by procedures discussed

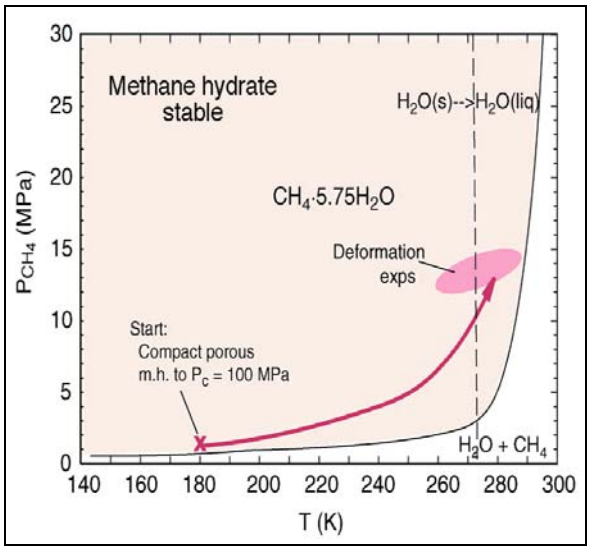

Figure 1. Temperature-pressure conditions during compaction and deformation testing of methane hydrate (m.h.) samples. CH_4 pore pressure is kept on samples to maintain them within their nominal equilibrium stability field, while external confining pressure is incrementally stepped to 100 MPa. Final compaction is performed at T > 273 K to melt and eliminate any ice that may be produced in samples during handling, jacketing, or cold compaction procedures.

previously [21] and reviewed elsewhere in this volume [22]. Briefly, small sections of samples were cleaved under liquid nitrogen from the bulk samples, transferred to a sample stage within an evacuated and pre-chilled (T<100 K) cryo-preparation station (Gatan Alto Model 2100), which in turn attaches to the sample chamber of our LEO 982 field emission SEM. Sample sections were again cleaved under vacuum at T<100K, transferred directly to the SEM column, and imaged at T<100K, at 1-2kV, under vacuum below 10^{-5} mbar.

RESULTS AND DISCUSSION

Sample textures and grain morphology. Figure 2 shows some examples of textural progression and grain structure evolution accompanying gas hydrate formation from granular ice under high-pressure high-temperature conditions, and the pronounced changes resulting from compaction and deformation testing. We reported previously [21] on the surprising finding that methane hydrate initially develops as a highly mesoporous material that nucleates at exposed ice surfaces, forming sharply defined boundaries with the dense ice reactant (Figs. 3 and 4 in [22] *this volume*; see also [23-26]). The early-

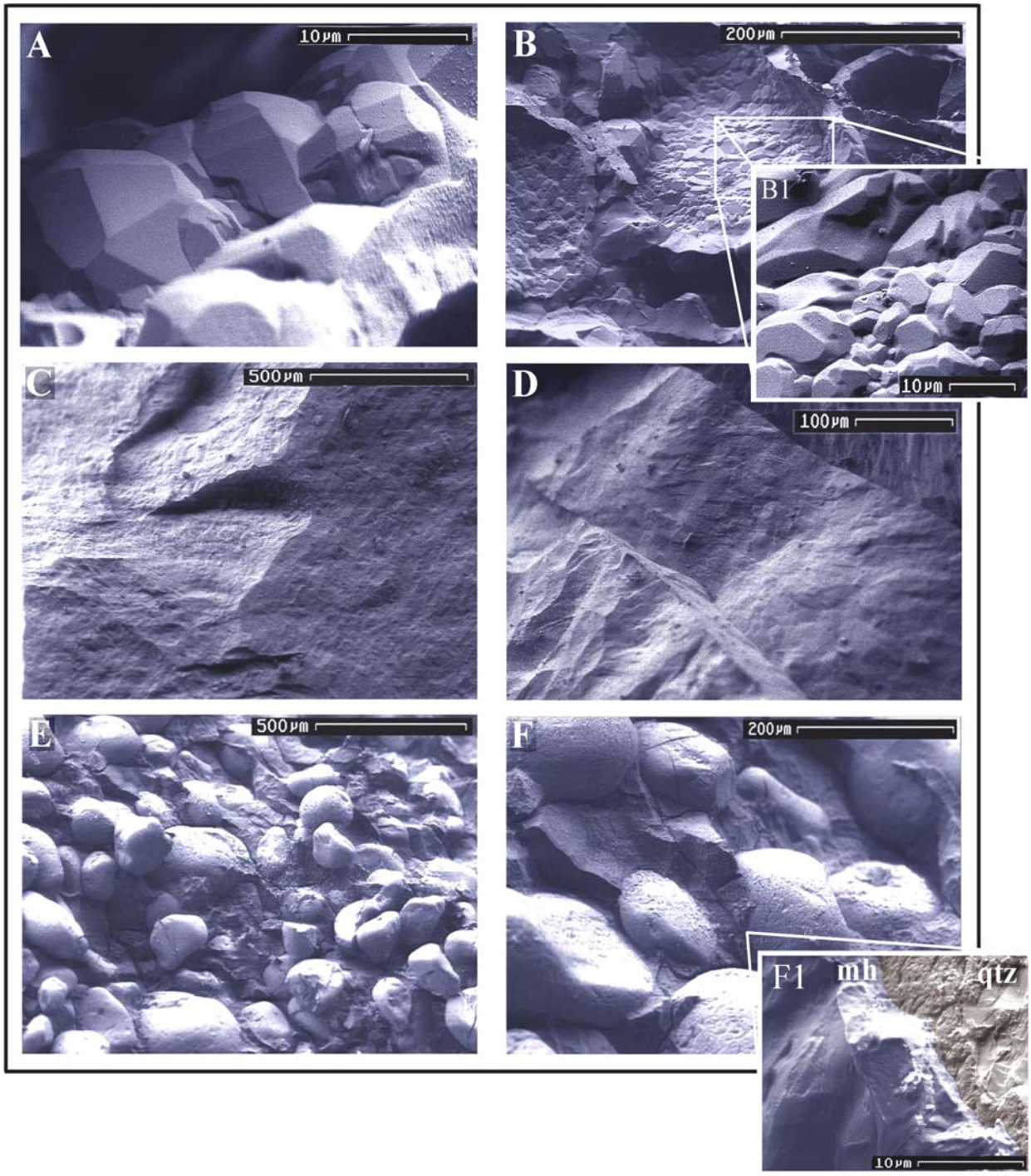

Figure 2. Textural progression of samples, starting as densely crystalline "as grown" gas hydrate to the massive and fine grained material observed after compaction and rheological testing. Image **A** shows the highly crystalline appearance of methane hydrate ("as grown"), after reaction from ice + gas at elevated pressures and temperatures. Images **B** and **B1** (inset) show CO_2 hydrate exhibiting similar development of fully formed hydrate grains lining exposed pore or cavity walls (see text for further discussion.). Image **C** shows the massive appearance of fully compacted pure methane hydrate, and **D** shows compacted pure CO_2 hydrate. Photos **E**, **F**, and **F1** show various magnification images of a 50/50 by volume methane hydrate + quartz sample after compaction and rheological testing. In **F1**, methane hydrate and quartz are labeled "mh" and "qtz" respectively. This image shows that the hydrate retains its material density as seen in **A**, **B**, and **B1**, yet individual grain boundaries within the hydrate are difficult to discern.

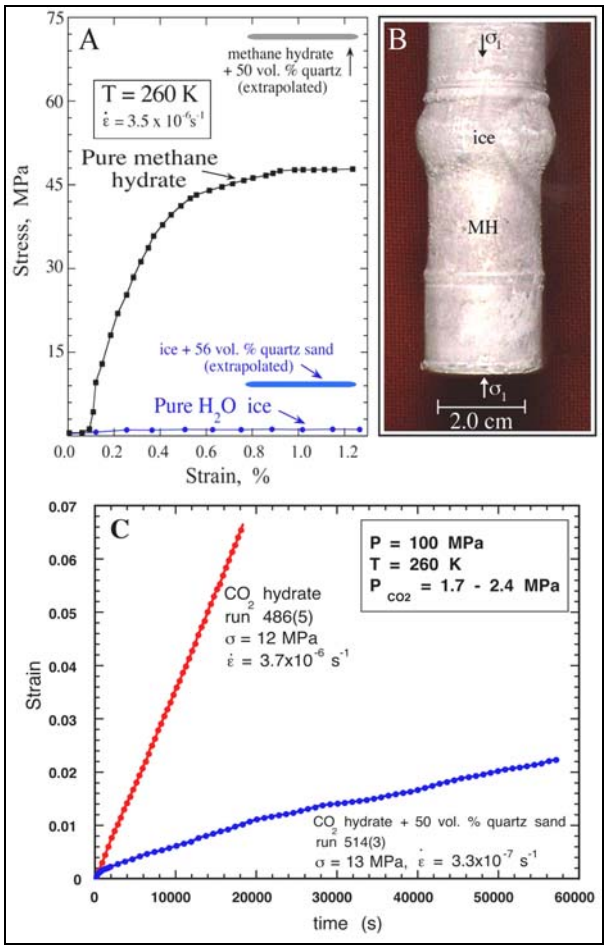

Figure 3. **A** and **B:** Manifestations of the exceptional strength contrast between pure methane hydrate and pure water ice. **A** shows stress-strain curves for samples of pure methane hydrate *vs*. ice, each tested at 260 K with confining pressure 100 MPa, at strain rate of $3.5x10^{-6}$ s^{-1}. Under these conditions, methane hydrate is roughly 30 times stronger than ice, and this strength contrast continues to increase with decreasing temperature (Fig. 4). The extrapolated steady-state stress for samples of methane hydrate + 50 vol. % quartz sand (sample shown in Fig. 2E and F), and for ice + 56 vol. % quartz sand are also shown for comparison. The mixed-phase aggregates were tested at conditions just above and below 260 K, hence the extrapolation. **B**: Indium-jacketed composite sample of ice (top) and methane hydrate ("MH", bottom) after deformation. The sample was a near-perfect cylinder prior to testing. The post-test appearance of the sample shows that virtually all the sample strain is accommodated in the (weaker) ice phase. Fig. 3A is modified from figures discussed in greater detail in [10, 11]. **C:** Creep of CO_2 hydrate *vs*. CO_2 hydrate + quartz sand under nearly matching experimental conditions. Every 3rd data point is plotted. Creep is defined as deformation under conditions of constant stress; in contrast, the data in **A** were measured under conditions of constant imposed strain rate. At steady-state, the two measurement methods are equivalent. The pure material flows approximately one order of magnitude faster than the 50:50 sand mixture.

formed hydrate then continues to develop as thick-walled, spherical-to-irregular shaped shell-like structures that presumably mark the locations of original ice grains ([21]; see also Fig. 5 in [22]). Some ice melting and formation of hydrate from the liquid phase occurs concurrently, the proportion of which can vary depending on formation conditions. Progressive annealing then accompanies late-stage reaction at peak *P-T* conditions, typically producing dense, well-crystallized material that exhibits little to no mesoporosity (Fig. 2A, B; see also [22]).

The final "as-grown" sI and sII gas hydrates typically display fully formed cubic crystals, some with facets lining open cavities. Representative images of methane and CO_2 hydrate are shown in Figure 2 A and B. Intergranular porosity in final samples is typically 30%, and shows far more complex geometrical shapes and connectivity than the relatively simple pore geometry between the original near-spherical ice grains [21, 22]. The volumetric increase of the H_2O structure, local recrystallization, and associated rearrangement of the H_2O phase contributes to the substantial changes in pore geometry during the conversion of ice (± liquid water) to hydrate [21, 22].

The crystalline state developed within the as-grown porous samples is lost during compaction and/or deformation procedures, giving the fully dense material a massive appearance in which hydrate grain outlines are difficult to identify (Fig. 2C and D). In the fully dense hydrate/sediment aggregates, the hydrate phase forms a strong cement between sediment grains. When the proportion of hydrate is relatively high, such as in the 50:50 by volume hydrate:quartz sample shown in Figure 2 E and F, the hydrate forms a dense, load-bearing matrix that often encloses each sand grain. Higher magnification (Fig. 2 F1) shows that the hydrate retains its material density and is not mesoporous, yet hydrate-to-hydrate grain boundaries are virtually impossible to resolve (compare Fig. 2 F1 to B1).

Rheological comparisons of gas hydrates, ice, and sediment mixtures. The exceptional strength contrast between pure gas hydrate or gas hydrate-bearing sediment, compared with pure water ice or with ice + sand mixtures, is shown in Figures 3 and 4. The strength contrast between methane hydrate and ice is shown both quantitatively and qualitatively in Fig. 3A,B and direct comparisons of the strength of CO_2 hydrate and CO_2 hydrate + quartz are shown in Fig. 3C.

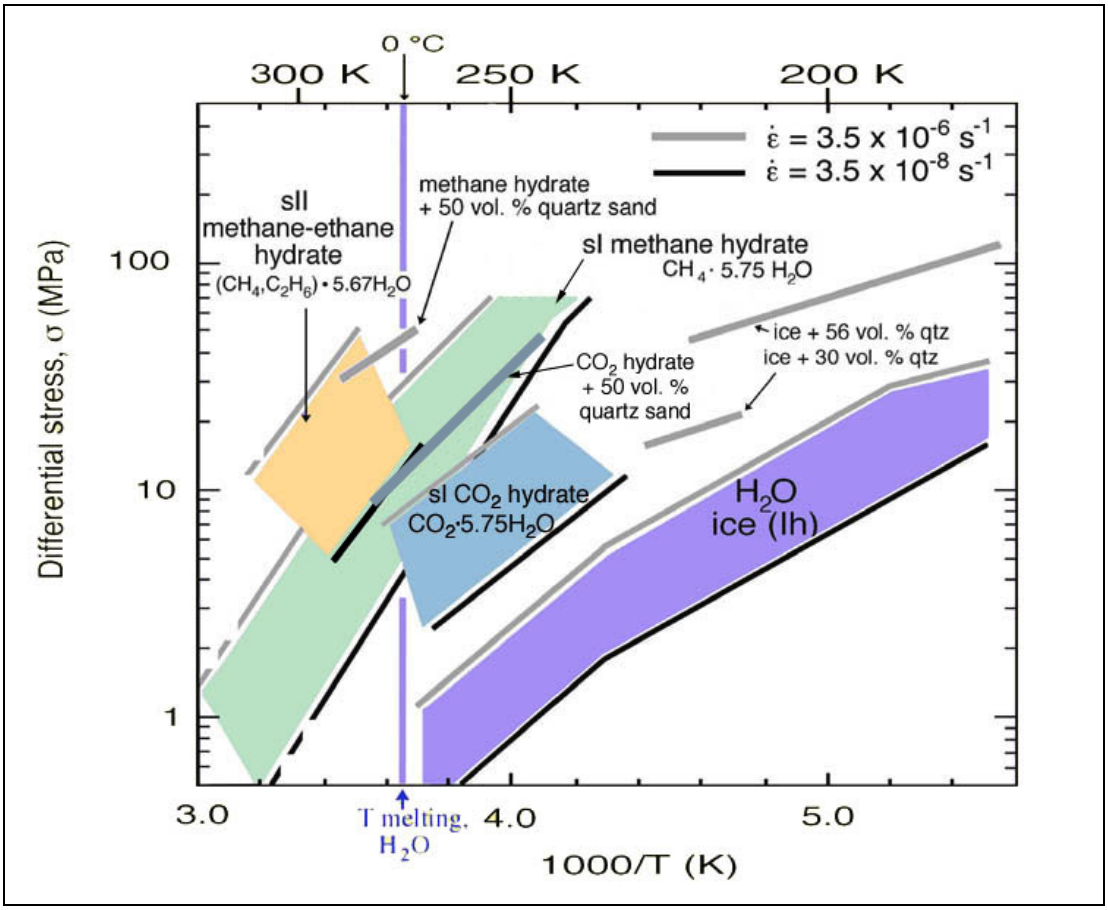

Figure 4. Comparison of ductile flow behavior, plotted as log σ *vs.* 1/T, of methane hydrate + quartz sand mixed aggregate (50/50 vol. %) and CO_2 hydrate + quartz sand (~ 50/50 vol. %), in relation to pure sI methane hydrate (data from [10] and [11]), sI CO_2 hydrate [12], sII methane-ethane hydrate [12], pure water ice [18] and comparable ice + quartz sand mixtures [19] made with the same quartz sand standard as that used in the methane hydrate or CO_2 hydrate + sand tests. Strain rates for end-member materials shown here range 3.5 x $10^{-6}s^{-1}$ to 3.5 x $10^{-8}s^{-1}$, and mixed-phase aggregates are shown at 3.5 x $10^{-6}s^{-1}$. Confining pressure for all gas hydrate tests was 50 MPa. These results illustrate that not only are gas hydrates substantially stronger than water ice, but measurable differences in strength are apparent between the different structures of hydrate (sI methane hydrate *vs.* sII methane-ethane hydrate) as well as between different compositions of the same structure (sI methane *vs.* sI CO_2 hydrate). Adding a secondary hard phase has additional strengthening effects, as discussed in the text.

The stress-strain curves shown in Fig. 3A measured on pure methane hydrate samples and pure H_2O ice at 260 K, show that at strain rate of 3.5x10^{-6} s^{-1}, methane hydrate is roughly 30 times stronger than ice. This strength contrast then continues to increase with decreasing temperature (Figure 4). The extrapolated steady-state stress for samples of methane hydrate + 50 vol. % quartz sand (sample shown in Fig. 2E and F), and for ice + 56 vol. % quartz sand (using the same quartz sand standard) are also shown in Figure 3A for comparison to pure methane hydrate and pure ice, for simple comparisons of stress *vs.* strain.

Other notable results are shown in Figure 4, including the very high plastic flow strength of all gas-hydrate-bearing materials we have measured to-date, compared to water ice. At 263 K and strain rate 3.5 x $10^{-6}s^{-1}$, for example, the steady-state stress supported by polycrystalline water ice is only about 1.5 MPa, compared with ~ 10 MPa for CO_2 hydrate, ~ 38 MPa for methane hydrate, and close to 100 MPa (extrapolated) for sII methane-ethane hydrate.

Figure 4 also shows that adding a nearly homogeneous distribution of ~ 50 vol. % quartz to

either methane hydrate or CO_2 hydrate serves to increase the strength by about a factor of two with respect to the pure hydrate. This effect appears to be roughly comparable, although somewhat less pronounced, than the effect of adding the same quartz sand standard to pure ice. As shown in Figure 4, the addition of 30 vol.% quartz sand to ice results in about a 2.5 to 3x strength increase, and the addition of 56% quartz sand nearly doubles this strength increase. Further testing is needed to determine whether the addition of particulates to gas hydrates also has a similar "toughening" or other work-hardening effect as that exhibited by ice/sediment mixtures [19].

Lastly, Figure 4 illustrates that while the end-member gas hydrates are markedly stronger than ice, there are significant differences between at least some sI and sII hydrocarbon hydrates. Furthermore, different compositions of the same-structure hydrate (sI methane *vs.* sI CO_2 hydrate, for instance) can also exhibit different rheologies.

IMPLICATIONS AND CONCLUSIONS

The high strength of gas hydrates has implications for hydrate-bearing formations in nature even where hydrate concentrations are low. If environmental conditions permit high effective normal stresses (high confining pressure relative to pore pressure), frictional resistance and cohesion between sediment grains may be high enough that time-dependent plastic deformation within the weakest grains of the aggregate governs macroscopic strength. In the case of methane-hydrate-bearing sediment formations, it is the hydrate that is the weakest phase, and the strength of the hydrate phase may thus have a markedly different effect than previously expected.

The high strength of gas hydrates also implies a much higher flow strength for hydrate + sediment aggregates compared with that of frozen soils. This conclusion is further supported by the test results from the 50/50 methane hydrate + quartz sample and the 50/50 CO_2 hydrate + quartz sample, although additional testing is needed to demonstrate reproducibility and to fully explore the many effects and complexities that sediments, in different sizes, concentrations, and distributions, may introduce. Nonetheless, these first tests on a hydrate/sediment mixture demonstrates that adding a nearly homogeneous distribution of ~ 50 vol. % quartz to methane or CO_2 hydrate serves to increase the strength by about a factor of two compared to the pure hydrate.

Lastly, the significant differences between the various compositions of gas hydrates is quite notable given the long-held assumptions in the literature that hydrates are likely "ice-like" in their mechanical properties, or could be compared to analogue hydrates easily formed in the laboratory (ethylene oxide or THF hydrates, for instance). To the contrary, we now know that guest species can critically influence many physical properties and behaviors exhibited by clathrate hydrates, an example being the startling difference in decomposition behavior exhibited by various sI and sII hydrates [27, also 17]. Mechanical strength is no different; Figure 4 illustrates that not only do sI and sII hydrates exhibit significantly different rheologies, but different compositions of the same hydrate structure can exhibit different rheologies.

These experiments represent merely a first step towards elucidating the mechanical effects of gas hydrates on hydrate-bearing formations. Planned experiments on compaction, fracture, and flow behavior of hydrate + sediment aggregates with known phase articulation, or under conditions of controlled dissociation, should further improve our understanding of the specific roles that gas hydrate rheology may play in governing the inelastic behavior of natural hydrate/sediment aggregates. In complementary manner, SEM imaging should then help relate the lab measurements to those made on either recovered or *in situ* gas-hydrate-bearing materials, and in turn, to appropriate rock-physics models.

AKNOWLEDGMENTS.

This work was supported in part by the USGS Gas Hydrate Project and NASA's Planetary Geology and Geophysics Program. We thank W. Waite and J. Pinkston of the USGS for helpful reviews of the manuscript. Work by WBD was performed under the auspices of the U.S. Department of Energy by the Lawrence Livermore National Laboratory under contract W-7405-ENG-48.

REFERENCES

[1] Holbrook, W., Hoskins, H., Wood, W., Stephen, R., Lizarralde, D. and Leg 164 Science Party. *Methane hydrate and free gas on the Blake Ridge from vertical seismic profiling.* Science 1996; 273:1840-1843.

[2] Dallimore, S., and Collett, T. *Scientific results from JAPEX/JNOC/GSC Malllik 2L-38 gas hydrate research well, Mackenzie Delta, Northwest Territories, Canada*. T. Collett, editor. Geological Survey of Canada, Ottawa, Ont., p. 31, 1999.

[3] Martinson, O. *Mass movements*. In: Maltman A., editor. Geological deformation of sediments. London: Chapman & Hall. London, 1994. p. 127-165.

[4] Andersland, O., and Ladanyi, B. Frozen ground engineering. Chapman & Hall, New York, 1994.

[5] Handy, M. *Flow laws for rocks containing two non-linear viscous phases: a phenomenological approach*. Journal of Structural Geology 1994; 16 (3): 287-301.

[6] Tullis, T., Jorowitz, G., and Tullis, J. *Flow laws of polyphase aggregates from end-member flow laws*. Journal of Geophysical Research 1991; 96:8081-8096.

[7] Circone, S., Stern, L., Kirby, S., Pinkston, J., and Durham, W. *Methane hydrate dissociation rates at 0.1 MPa and temperatures above 272 K*. In: Gas Hydrates: Challenges for the Future, Ed by G. Holder and P. Bishnoi, Annals of the New York Academy of Sciences 2000; 912:544-555.

[8] Peters, D., Selim, M., and Sloan, E.D. *Hydrate dissociation in pipelines by two-sided depressurization*. In: G. Holder and P. Bishnoi, eds. Gas Hydrates: Challenges for the Future. Annals of the New York Academy of Sciences 2000; 912: 304-313.

[9] Sloan, E. D. Jr. *Clathrate hydrates of natural gases (revised edition*). New York: Marcel Dekker, Inc., 1998.

[10] Durham, W., Kirby, S., Stern, L., and Zhang, W. *The strength and rheology of methane clathrate hydrate.* Journal of Geophysical Research 2003; 108(B4):2182-2193.

[11] Durham, W., Stern, L., and Kirby, S. *Ductile flow of methane hydrate*. Canadian Journal of Physics 2003; 81(1-2): 373-380.

[12] Durham, W., Stern, L., and Kirby, S. *The rheology of clathrate hydrates and its relation to planetary ice*. SMEC (Study of Matter at Extreme Conditions) conference abstracts, March 24-28, Miami, 2003.

[13] Helgerud, M. B. *Wavespeeds in gas hydrate and sediments containing gas hydrate: A laboratory and modeling study*. Ph.D. thesis, Stanford University, 2001.

[14] Helgerud, M., Waite, W., Kirby, S., and Nur, A. *Measured temperature and pressure dependence of compressional and shear wave speeds in polycrystalline sI methane hydrate and polycrystalline ice Ih*. Proceedings of the 4th International Conference on Gas Hydrates, Yokohama Japan, 2002; 711-715.

[15] Stern, L., Kirby, S., and Durham, W. *Peculiarities of methane clathrate hydrate formation and solid-state deformation, including possible superheating of water ice*. Science 1996; 273: 1843-1848.

[16] Stern, L., Kirby, S., Durham, W., Circone, S., and Waite, W. *Synthesis of pure methane hydrate suitable for measurement of physical properties and decomposition behavior.* Chapter 25 in: M.D. Max, editor. Natural Gas Hydrate In Oceanic and Permafrost Environments. Dordrecht: Kluwer, 2000. p. 323-346.

[17] Circone, S., Stern, L., Kirby, S., Durham, W., Chakoumakos, B., Rawn, C.J., Rondinone, A., and Ishii, Y. *CO_2 hydrate: synthesis, composition, dissociation behavior, and a comparison to structure I CH_4 hydrate*. Journal of Physical Chemistry B 2003; 107(23): 5529-5539.

[18] Durham, W. and Stern, L. *Rheological properties of water ice – Applications to satellites of the outer planets*. Ann. Rev. Earth & Planetary Sciences 2001; 29:295-330.

[19] Durham, W., Kirby, S., and Stern, L. *Effects of dispersed particulates on the rheology of water ice at planetary conditions.* Journal of Geophysical Research 1992; 97(E12): 20,883-20,897.

[20] Circone, S., Kirby, S.H., Pinkston, J.C., and Stern, L.A., *Measurement of gas yields and flow rates using a custom flowmeter*. Review of Scientific Instruments 2001; 72(6): 2709-2716.

[21] Stern, L., Circone, S., Kirby, S., and Durham, W. *Application of Scanning Electron Microscopy (SEM) to investigate growth and annealing of gas clathrate hydrates formed from melting ice.* American Mineralogist 2004; 89(8-9):1162-1175.

[22] Stern, L., Circone, S., Kirby, S., and Durham, W., *SEM imaging of gas hydrate formation processes and growth textures, and comparison to natural hydrates of marine and permafrost origin.* Proceedings of ICGH 2005, this volume.

[23] Kuhs, W., Klapproth, A., Gotthardt, F., Techmer, K., and Heinrichs, T. *The formation of meso- and macroporous gas hydrates.* Geophysical Research Letters 2000; 27:2929-2932.

[24] Staykova, D., Kuhs, W., Salamatin, A., and Hansen, T. *Formation of porous gas hydrate from ice powders: diffraction experiments and multi-stage model*. Journal of Physical Chemistry B 2003; 107:10299-10311.

[25] Klapproth, A., Goreshnic, E., Staykova, D., Klein, H., and Kuhs, W. *Structural studies of gas hydrates*. Canadian Journal of Physics 2003; 81(1-2):503-518.

[26] Genov, G., Kuhs, W., Staykova, D., Goreshnik, E., and Salamatin, A. *Experimental studies of the formation of porous gas hydrates*. American Mineralogist 2004; 89 (8-9): 1228-1239.

[27] Stern, L., Circone, S., Kirby, S., and Durham, W., *Temperature, pressure, and compositional effects on anomalous or "self" preservation of gas hydrates*. Canadian Journal of Physics 2003; 81(1-2):271-283.